

( $\sigma \approx 0.003\text{--}0.015$  mag), almost any transit-like light curve can be reproduced as a blend, and only with spectroscopy can these cases be recognized. For each trial simulation, the relative brightness and velocity amplitude of the primary in the eclipsing binary can be predicted. Although a good fit to the photometry of OGLE-TR-56 can indeed be obtained for a model with a single star blended with a fainter system comprising a G star eclipsed by a late M star, the G star would be bright enough that it would introduce strong line asymmetries (which are not seen), or would be detected directly by the presence of a second set of lines in the spectrum. Careful inspection using TODCOR<sup>18</sup> rules this out as well. Therefore, based on the data available, a blend scenario seems extremely unlikely.

This is the faintest ( $V \approx 16.6$  mag) and most distant ( $\sim 1,500$  pc) star around which a planet with a known orbit has been discovered. The planet is quite similar to the only other extrasolar giant planet with a known radius, HD209458b, except for having an orbit which is almost two times smaller. Thus its substellar hemisphere can heat up to about 1,900 K. However, this is still insufficient to cause appreciable planet evaporation (with a thermal root-mean-square (r.m.s.) velocity for hydrogen of around  $7\text{ km s}^{-1}$  compared to a surface escape velocity of around  $50\text{ km s}^{-1}$ ). The tidal Roche lobe radius of OGLE-TR-56b at its distance from the star is about 2 planet radii. The planet's orbit is most probably circularized ( $e = 0.0$ ) and its rotation tidally locked, but the star's rotation is not synchronized ( $v \sin i \approx 3\text{ km s}^{-1}$ ). Thus the system appears to have adequate long-term stability. Interestingly, OGLE-TR-56b is the first planet found in an orbit much shorter than the current cut-off of close-in giant planets at 3–4-day periods ( $\sim 0.04\text{ AU}$ )<sup>8</sup>. This might indicate a different mechanism for halting migration in a protoplanetary disk. For example, OGLE-TR-56b may be representative of a very small population of objects—the so-called class II planets, which have lost some of their mass through Roche lobe overflow<sup>21</sup> but survived in close proximity to the star; a detailed theoretical study of OGLE-TR-56b will be presented elsewhere (D.D.S., manuscript in preparation). These observations clearly show that transit searches provide a useful tool in adding to the great diversity of extrasolar planets being discovered. □

Received 27 November; accepted 30 December 2002; doi:10.1038/nature01379.

1. Charbonneau, D., Brown, T. M., Latham, D. W. & Mayor, M. Detection of planetary transits across a Sun-like star. *Astrophys. J.* **529**, L45–L48 (2000).
2. Henry, G. W., Marcy, G. W., Butler, R. P. & Vogt, S. S. A transiting “51 Peg-like” planet. *Astrophys. J.* **529**, L41–L44 (2000).
3. Mazeh, T. *et al.* The spectroscopic orbit of the planetary companion transiting HD 209458. *Astrophys. J.* **532**, L55–L58 (2000).
4. Udalski, A. *et al.* The optical gravitational lensing experiment. Search for planetary and low-luminosity object transits in the Galactic disk. Results of 2001 campaign. *Acta Astron.* **52**, 1–37 (2002).
5. Udalski, A. *et al.* The optical gravitational lensing experiment. Search for planetary and low-luminosity object transits in the Galactic disk. Results of 2001 campaign – Supplement. *Acta Astron.* **52**, 115–128 (2002).
6. Mayor, M. & Queloz, D. A Jupiter-mass companion to a solar-type star. *Nature* **378**, 355–359 (1995).
7. Marcy, G. W. & Butler, R. P. Detection of extrasolar giant planets. *Annu. Rev. Astron. Astrophys.* **36**, 57–98 (1998).
8. Schneider, J. *The Extrasolar Planet Encyclopaedia*, available at <http://www.obspm.fr/encycl/encycl.html> (2002).
9. Wolszczan, A. & Frail, D. A. A planetary system around the millisecond pulsar PSR1257 + 12. *Nature* **355**, 145–147 (1992).
10. Jha, S. *et al.* Multicolor observations of a planetary transit of HD 209458. *Astrophys. J.* **540**, L45–L48 (2000).
11. Brown, T. M., Charbonneau, D., Gilliland, R. L., Noyes, R. W. & Burrows, A. Hubble space telescope time-series photometry of the transiting planet of HD 209458. *Astrophys. J.* **552**, 699–709 (2001).
12. Charbonneau, D., Brown, T. M., Noyes, R. W. & Gilliland, R. L. Detection of an extrasolar planet atmosphere. *Astrophys. J.* **568**, 377–384 (2002).
13. Brown, T. M., Libbrecht, K. G. & Charbonneau, D. A search for CO absorption in the transmission spectrum of HD 209458b. *Publ. Astron. Soc. Pacif.* **114**, 826–832 (2002).
14. Horne, K. in *Proc. Scientific Frontiers of Research on Extrasolar Planets* (eds Deming, D. & Seager, S.) (ASP, San Francisco, in the press).
15. Vogt, S. S., *et al.* in *Proc. SPIE Instrum. in Astronomy VIII* (eds Crawford, D. L. & Craine, E. R.) 362–375 (SPIE, Bellingham, WA, 1994).
16. Tinney, C. G. *et al.* First results from the Anglo-Australian planet search: A brown dwarf candidate and a 51 Peg-like planet. *Astrophys. J.* **551**, 507–511 (2001).
17. Seager, S. & Mallén-Ornelas, G. On the unique solution of planet and star parameters from an extrasolar planet transit light curve. *Astrophys. J.* (submitted); preprint <http://arXiv.org/astro-ph/0206228> (2002).

18. Zucker, S. & Mazeh, T. Study of spectroscopic binaries with TODCOR. I: A new two-dimensional correlation algorithm to derive the radial velocities of the two components. *Astrophys. J.* **420**, 806–810 (1994).
19. Queloz, D. *et al.* No planet for HD 166435. *Astron. Astrophys.* **379**, 279–287 (2001).
20. Santos, N. C. *et al.* The CORALIE survey for southern extra-solar planets. IX. A 1.3-day period brown dwarf disguised as a planet. *Astron. Astrophys.* **392**, 215–229 (2002).
21. Trilling, D. E. *et al.* Orbital evolution and migration of giant planets: Modeling extrasolar planets. *Astrophys. J.* **500**, 428–439 (1998).
22. Cody, A. M. & Sasselov, D. D. HD 209458: Physical parameters of the parent star and the transiting planet. *Astrophys. J.* **569**, 451–458 (2002).

**Acknowledgements** We thank A. Udalski and the OGLE team for generous contributions to this project. We are very grateful to S. Kulkarni for support, to R. Noyes and D. Latham for comments, to T. Barlow for assistance with the spectroscopic reductions using the MAKEE Keck Observatory HIRES Data Reduction Software (<http://spider.ipac.caltech.edu/staff/tab/makee>) and to K. Stanek for his encouragement. The data presented here were obtained at the W.M. Keck Observatory (operated by Caltech, the University of California, and NASA), which was made possible by the generous financial support of the W. M. Keck Foundation. M.K. gratefully acknowledges the support of NASA through the Michelson Fellowship programme. G.T. acknowledges support from NASA's Kepler Mission. S.J. thanks the Miller Institute for Basic Research in Science at UC Berkeley for support via a research fellowship.

**Competing interests statement** The authors declare that they have no competing financial interests.

**Correspondence** and requests for materials should be addressed to M.K. (e-mail: [maciej@gps.caltech.edu](mailto:maciej@gps.caltech.edu)).

## Long-distance teleportation of qubits at telecommunication wavelengths

I. Marcikic\*†, H. de Riedmatten\*†, W. Tittel\*‡, H. Zbinden\* & N. Gisin\*

\* Group of Applied Physics, University of Geneva, CH-1211 Geneva 4, Switzerland  
 ‡ Danish National Research Foundation Center for Quantum Optics (QUANTOP), Institute for Physics and Astronomy, University of Aarhus, Denmark

† These authors contributed equally to this work

Matter and energy cannot be teleported (that is, transferred from one place to another without passing through intermediate locations). However, teleportation of quantum states (the ultimate structure of objects) is possible<sup>1</sup>: only the structure is teleported—the matter stays at the source side and must be already present at the final location. Several table-top experiments have used qubits<sup>2–7</sup> (two-dimensional quantum systems) or continuous variables<sup>8–10</sup> to demonstrate the principle over short distances. Here we report a long-distance experimental demonstration of probabilistic quantum teleportation. Qubits carried by photons of 1.3 μm wavelength are teleported onto photons of 1.55 μm wavelength from one laboratory to another, separated by 55 m but connected by 2 km of standard telecommunication fibre. The first (and, with foreseeable technologies, the only) application of quantum teleportation is in quantum communication, where it could help to extend quantum cryptography to larger distances<sup>11–13</sup>.

Since the first article presenting the concept<sup>1</sup> (Fig. 1), quantum teleportation has received much attention. On the conceptual side, it has been proved to be a universal gate for quantum computing<sup>14</sup>. In particular, together with quantum memories, it offers the possibility of realizing quantum repeaters with unlimited range<sup>15</sup>. But it is fair to say that the fundamental meaning of quantum teleportation for our understanding of quantum nonlocality (and of the structure of space and time) may still be awaiting discovery. On the experimental side, progress in demonstrating the concept has been surprisingly fast. In 1997, two groups—one in Rome, one in Innsbruck—presented results of quantum teleportation using qubits. The Italian group<sup>2</sup> teleported a qubit carried by one of the

photons of an entangled photon pair. However, this approach prevents the possibility of concatenating this teleportation scheme. The Austrian group<sup>3</sup> used a more complete scheme, where only one qubit is carried per photon. In fact, soon after their initial experiment they demonstrated entanglement swapping<sup>16,17</sup>—that is, the teleportation of an entangled qubit. However, this scheme was also incomplete, as it used what is called a partial Bell-state measurement, which implies that (even in principle) the teleportation succeeds only in 25% of cases. A few years later a teleportation experiment with complete Bell-state measurements was presented<sup>5</sup>, but the efficiency of the measurement was only of the order of  $10^{-10}$ .

The difficulty is that a complete Bell-state measurement for qubits requires nonlinear optics<sup>18</sup>. Hence, one uses linear optics and accepts incomplete measurements, or uses nonlinear optics and accepts very inefficient measurements; or one does not use qubits, or finite dimensional Hilbert spaces. Indeed, it has been shown, first theoretically<sup>19</sup>, then experimentally<sup>8</sup>, that the teleportation of continuous variables can, in principle, be fully achieved using linear optics. However, the difficulty is then to produce close to maximally entangled states. This difficulty is even more significant when the distance is increased, because squeezed states of light beams (that is, entangled states for continuous variables) are very vulnerable to losses.

Here we report an experimental long-distance demonstration of quantum teleportation. Qubits carried by photons of  $1.3\ \mu\text{m}$  wavelength are teleported onto photons of  $1.55\ \mu\text{m}$  wavelength from one laboratory to another, separated by 55 m, but connected by 2 km of standard telecommunication fibre. Our experiment follows the line of the Austrian group, in that we use linear optics for our partial Bell-state measurement. However, it also differs significantly in that our qubits and necessary entangled states are not encoded in polarization, but in superposition and entanglement of time-bins<sup>20,21</sup>, respectively (Fig. 2). This kind of encoding is more robust against decoherence in optical fibres<sup>22</sup>. Moreover, we use two nonlinear crystals, which is necessary for the implementation of quantum communication protocols where space-like separation of the photon pair sources is required<sup>15</sup>.

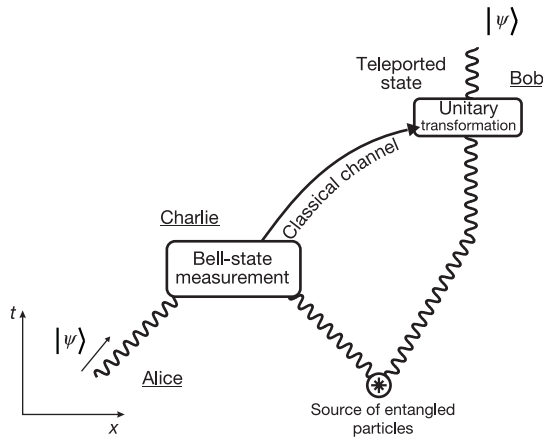


**Figure 1** Space–time diagram of a general quantum teleportation scheme. Axes are given in the lower left corner. Alice holds a quantum system in an unknown state that she wishes to transmit to Bob. However, she can not send the particle directly, perhaps because of a lossy transmission channel. She decides to send her quantum state via Charlie, who shares a pair of entangled particles and a classical communication channel with Bob. Charlie now entangles Alice’s particle with his part of the shared pair by means of a so-called Bell-state measurement, and then communicates the result—that is, the Bell state he projected onto—to Bob. Bob then performs a unitary transformation, depending on Charlie’s result, and Bob’s particle finally carries precisely the quantum state of Alice’s initial particle. Note that the Bell-state measurement destroys the quantum state of the initial particle, and that no information about which state is teleported is acquired, because its final state is completely mixed.

Our experimental set-up is presented in Fig. 3. A femtosecond laser beam is split into two parts by a variable beam-splitter. The transmitted beam is used to create entangled time-bin qubits that are shared between Charlie and Bob. The entangled state is described by:

$$|\Phi\rangle = \frac{1}{\sqrt{2}}(|1,0\rangle_{\text{Charlie}}|1,0\rangle_{\text{Bob}} + e^{i\varphi}|0,1\rangle_{\text{Charlie}}|0,1\rangle_{\text{Bob}}) \quad (1)$$

where  $|1,0\rangle$  represents the first time-bin and  $|0,1\rangle$  the second one. The imbalance of the pump interferometer defines the reference time difference  $\Delta\tau$  between the first and the second time-bin, thus the phase  $\varphi$  is taken to be zero.

The reflected beam is used to create the qubits to be teleported:

$$|\Psi\rangle_{\text{Alice}} = a_0|1,0\rangle_{\text{Alice}} + a_1e^{i\alpha}|0,1\rangle_{\text{Alice}} \quad (2)$$

where  $a_0 = 0, 1$  or  $1/\sqrt{2}$ , depending on the discrete variable coupler setting, and  $a_1 = \sqrt{1 - a_0^2}$ . The phase  $\alpha$  is defined relative to the reference phase  $\varphi$ . Alice’s qubit  $|\Psi\rangle_{\text{Alice}}$  is finally sent to Charlie.

Charlie performs the joint Bell-state measurement between the qubit sent by Alice and his part of the pair, using the 50/50 fibre beam-splitter (BS). Therefore, only two out of the four different results can be discriminated in principle<sup>18</sup>. We choose to select only

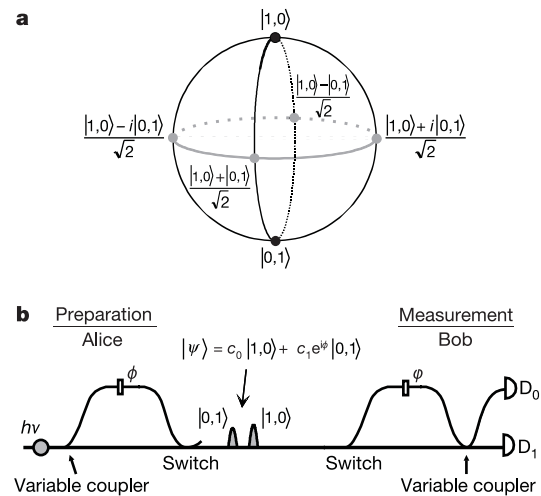


**Figure 2** Principle of preparation and measurement of time-bin qubits. **a**, Two time-bins constitute the basic states, denoted  $|1,0\rangle$  and  $|0,1\rangle$ . They are represented on the north and south pole of the Poincaré sphere. Their equal superpositions  $|1,0\rangle + e^{i\varphi}|0,1\rangle$  are represented on the equator. **b**, A time-bin qubit is an arbitrary superposition of two time-bins  $c_0|1,0\rangle + c_1e^{i\varphi}|0,1\rangle$ . This state corresponds to the input photon  $h\nu$  (left) passing through the short arm  $|1,0\rangle$  of an unbalanced interferometer, with probability amplitude  $c_0$ , and through the long arm  $|0,1\rangle$ , with probability amplitude  $c_1$ . The phase  $\phi$  (longitude on the qubit sphere) characterizes the imbalance of the interferometer with respect to a reference optical path length difference. Alice’s variable coupler sets the value of the two amplitudes (latitude on the qubit sphere), and the switch enables their lossless superposition (in principle). The right-hand side shows how arbitrary (projective) measurements can be implemented: Bob’s switch is used to send the first time-bin through the long arm, and the second time-bin through the short arm such that they arrive simultaneously at the variable coupler. The photon is then detected by one of two detectors,  $D_0$  or  $D_1$ . With the phase shifter and the variable coupler, the state can be measured in any basis<sup>20</sup>. Instead of using a true variable coupler, we use three different settings with coupling ratios of 0%, 100% and 50%. These settings correspond to preparation of and projection onto the states represented on the north pole, south pole and on the equator of the generalized Poincaré sphere. We also replaced the switches by passive fibre couplers. This implies a 50% loss, both for the preparation and the measurement apparatus. As fast switches have even larger losses, our choice is the most practical one and does not affect the principle of the experiment. The result of the measurement for each basis can then be found by looking at the appropriate detection times<sup>29</sup>. Note that the concept of time-bins, unlike polarization, can easily be generalized to higher dimensions<sup>30</sup>.

the one that projects the two particles onto the singlet entangled state:

$$|\Psi^-\rangle = \frac{1}{\sqrt{2}}(|1,0\rangle_{\text{Alice}}|0,1\rangle_{\text{Charlie}} - |0,1\rangle_{\text{Alice}}|1,0\rangle_{\text{Charlie}}) \quad (3)$$

This takes place when the two photons trigger the detectors labelled  $C_1$  and  $C_2$  in Fig. 3 at times that differ precisely by the time difference between two time-bins. Indeed, each of the two terms in equation (3) may produce this detection result, either with each photon remaining in its fibre or both coupling to the other (hence the  $\pi$  phase shift that corresponds to the minus sign in equation (3)). To achieve this projection, the two photons have to be indistinguishable when they emerge from the beam-splitter<sup>23</sup>.

The production of multiple pairs by the entangled photon source should be avoided in many quantum communication protocols<sup>24</sup>. If the probability of creating a photon pair is the same in both crystals, then, owing to stimulated emission, the probability of creating two pairs in one crystal is the same as the probability of creating one pair in each crystal<sup>25</sup>. Thus, two times out of three Charlie detects a wrong event<sup>23</sup>. In order to detect only the desired events, we

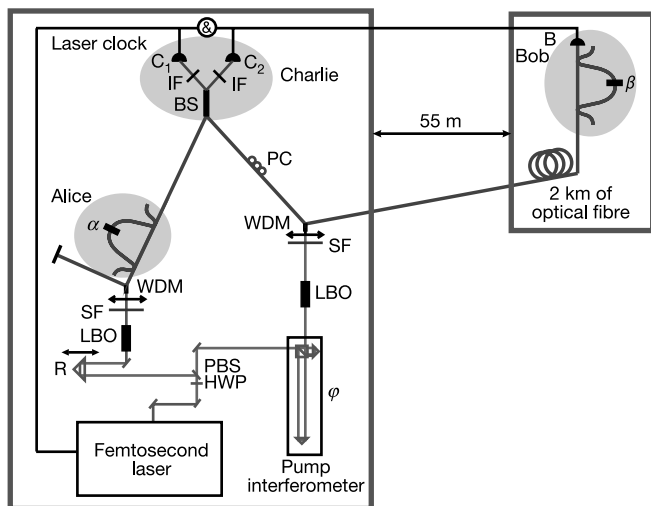


**Figure 3** Experimental set-up. Femtosecond laser pulses (with 150-fs pulse width at wavelength  $\lambda = 710$  nm, and 76-MHz repetition rate; Coherent Mira 900) are split into two parts using a variable beam-splitter made of a half-wave plate (HWP) and a polarizing beam-splitter (PBS). The reflected beam is used to produce the qubit to be teleported, and the transmitted beam is used to generate the necessary entangled qubit pair. For this purpose the reflected beam is first sent to a nonlinear crystal (lithium triborate, LBO, Crystal Laser), where, by parametric downconversion, a pair of twin photons at telecom communication wavelengths (1.31 and 1.55  $\mu\text{m}$ ) is created. Next, the pump light is removed with a silicon filter (SF), and the twin photons are collimated into an optical fibre and separated by a wavelength-division-multiplexer (WDM). The 1.55- $\mu\text{m}$  photon is ignored, and the 1.31- $\mu\text{m}$  photon is sent to Alice, who creates the time-bin qubits to be teleported (with a relative phase  $\alpha$ ), which she then forwards to Charlie. The retroreflector (R) is used to adjust the arrival time of Alice's qubit at Charlie's. The transmitted beam is first sent through an unbalanced Michelson bulk interferometer (with reference phase  $\varphi = 0$ ) and then through a similar nonlinear crystal, thus producing non-degenerate entangled time-bin qubits. The 1.31- $\mu\text{m}$  photon is sent to Charlie through a polarization controller (PC), and the 1.55- $\mu\text{m}$  photon is sent to Bob who is situated in another laboratory, 55 m away from Charlie and connected by 2 km of optical fibre. Charlie performs a partial Bell-state measurement on Alice's qubit and his part of the entangled pair, using the 50/50 fibre beam-splitter (BS). The photons are detected with single-photon detectors  $C_1$  and  $C_2$ . The interference filters (IF), centred at 1.31  $\mu\text{m}$  with spectral width of 10 nm, are used to render these two particles indistinguishable<sup>23</sup>. Finally, whenever the two-particles state is projected onto the  $|\Psi^-\rangle$  Bell state, Bob analyses his photon (using an interferometer with relative phase  $\beta$  and a single-photon detector B) to verify that the state encoded by Alice has indeed been teleported. The symbol '&' denotes coincidence detection of the different detector outputs.

decrease the probability of creating entangled qubits relative to the probability of creating the qubit to be teleported. The wrong events are thus reduced to only the cases where two entangled pairs are created; the number of such events can be made arbitrarily small. The ratio of probabilities is controlled by the variable coupler. Eventually, we chose a ratio of 8, with a probability of creating Alice's qubit per laser pulse of around 10%.

Bob is situated in another laboratory, 55 m away from Charlie. To simulate a longer distance, we added 2 km of standard dispersion shifted optical fibre before the teleported photon reaches Bob's analyser. Once Charlie has the information that the (partial) Bell-state measurement was successful, he informs Bob by the classical channel. This operation projects Bob's photon onto the state:

$$|\Psi\rangle_{\text{Bob}} = a_1 e^{i\alpha} |1,0\rangle_{\text{Bob}} - a_0 |0,1\rangle_{\text{Bob}} \quad (4)$$

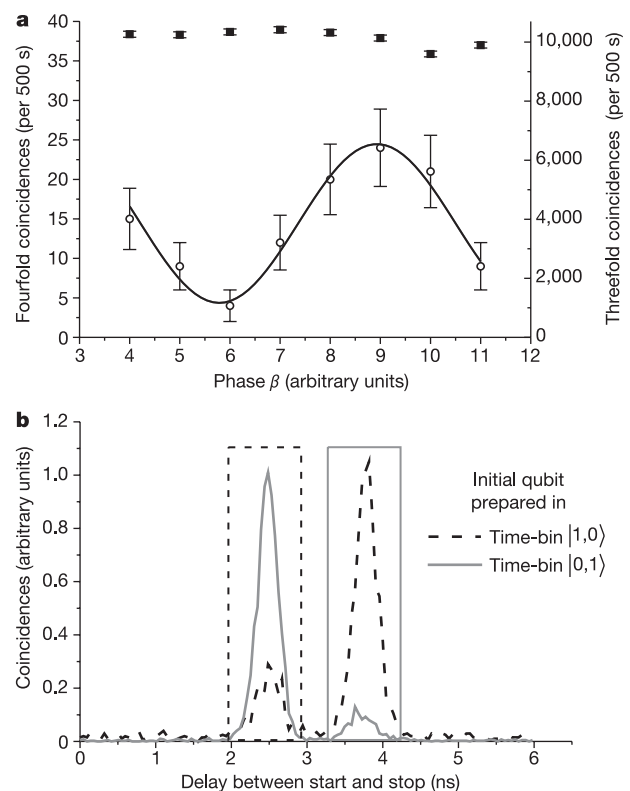


**Figure 4** Experimental results. **a**, Teleportation of a qubit consisting of a coherent superposition of two time-bins (equatorial states). Open circles represent Bob's count rate conditioned on the projection on the  $|\Psi^-\rangle$  Bell state (fourfold coincidences) as a function of the phase  $\beta$  in his interferometer. The clear interference pattern with visibility  $V = (70 \pm 5)\%$  confirms that teleportation takes place with a fidelity of  $(85 \pm 2.5)\%$ . Squares represent the three-fold coincidence count rates between laser pulse, one of Charlie's detectors ( $C_1$ ) and Bob's detector. They illustrate the stability of the set-up. **b**, Teleportation of qubits  $|1,0\rangle$  (north pole, dashed curve) and  $|0,1\rangle$  (south pole, plain curve). The corresponding fidelities are  $(77 \pm 3)\%$  and  $(88 \pm 3)\%$ , respectively. As indicated in equation (4), the projection onto the  $|\Psi^-\rangle$  Bell state leads to a bit-flip of the teleported state. The different results for the two input states are due to the fact that in our experimental set-up the detection of the first photon, in mode  $C_1$ , triggers the two other detectors,  $C_2$  and B. When we prepare the state  $|1,0\rangle$  the first detection is mostly due to Alice's photon, because as explained above, we produce eight times more qubits to be teleported than entangled pairs. Hence, the two detectors  $C_2$  and B are often triggered without any photon present, leading to an increasing number of accidental coincidences, that is, wrong events. When preparing the other state  $|0,1\rangle$ , the first detection in mode  $C_1$  can only be due to a photon coming from the source that generates entangled pairs, or to a dark count. As these events occur much less frequently than in the first-mentioned case, the corresponding teleportation fidelity is less affected by accidental coincidences.

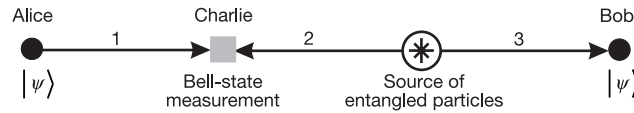


**Figure 5** Quantum teleportation used as a quantum relay. Quantum relays extend the range of quantum cryptography from tens of kilometres to hundreds of kilometres, though not to unlimited ranges. The basic idea is as follows<sup>11–13</sup>: in quantum cryptography, the noise is dominated by the detector dark counts; hence the noise is almost independent of the distance. The signal, however, decreases exponentially with distance because of the attenuation. With realistic numbers, this sets a limit close to 80 km. But if it were possible to verify at some points along the quantum channel whether or not the photon is still there, Bob could refrain from opening the detector when there is no photon. This simple idea is impractical, because it requires (at present

unrealistic) photon number quantum non-demolition measurements<sup>31</sup>. However, consider a channel divided into sections—for example, the three sections as illustrated here. Assume that the photon sent by Alice down the first section is teleported to Bob using the entangled photon pair generated between sections 2 and 3. Two photons travel towards Bob, and one towards Alice. But, because the time ordering of the measurements is irrelevant<sup>7</sup>, the logical qubit can be considered to propagate all the way from Alice to Bob. Accordingly, the Bell-state measurement and the two-photon source act on this logical qubit as a non-demolition measurement

In order to recover Alice’s qubit state (equation (2)), Bob should apply the  $\sigma_y$  unitary transformation, consisting of a bit flip ( $|1,0\rangle \leftrightarrow |0,1\rangle$ ) and a phase flip (of relative phase  $\pi$ ). However, these unitary operations are not necessary to prove that teleportation takes place.

To show that our teleportation set-up operates correctly, Bob analyses the received photon with an analyser adapted for the wavelength of 1.55  $\mu\text{m}$  (ref. 24; see Fig. 2). The analysis basis thus contains the vector:

$$k_0|1,0\rangle + k_1e^{i\beta}|0,1\rangle \quad (5)$$

where  $k_0 = 0,1$  or  $1/\sqrt{2}$ , depending on the variable coupler setting, and  $k_1 = \sqrt{1 - k_0^2}$ .

One of Charlie’s photons is detected by the passively quenched germanium avalanche photo diode (APD)  $C_1$  working at liquid nitrogen temperature in the so-called Geiger mode<sup>26</sup> (quantum efficiency  $\eta = 10\%$ , dark count rate d.c.r. = 35 kHz, from NEC). To reduce the noise we make a coincidence between the Germanium APD and a trigger from the laser pulses. The other photon arriving at Charlie’s and Bob’s photon are detected with Peltier-cooled InGaAs APDs ( $C_2$  and B, respectively) working in the so-called gated mode<sup>27</sup> ( $\eta = 30\%$ , d.c.r. =  $10^{-4}$  per ns, from id Quantique). The trigger is given by the coincidence between the germanium APD and the laser pulse. Finally, the signals of the APDs are sent to fast coincidence electronics. We monitor fourfold coincidences with a time-to-amplitude converter, where the start is given by a successful Bell-state measurement (detectors  $C_1$  and  $C_2$  + laser pulse) and the stop by Bob’s detector B. The start plays the role of the classical information that Charlie sends to Bob. We choose to record only the events when the photon in output  $C_2$  arrives with a time difference  $\Delta\tau$  after the photon in output  $C_1$ . We also record the coincidence between detectors  $C_1$  and B. The rate should remain constant, as it contains no information about the Bell-state measurement result. This provides a control of the stability of the entire set-up.

In order to show that our teleportation set-up is universal, we report the teleportation of two different classes of states. The first class is composed of superposition of two time-bins, and hence corresponds to state represented by points on the equator of the generalized Poincaré sphere (Fig. 2). The second class consists of the two time-bins themselves, represented by the north and south poles of the sphere. The quality of the teleportation is usually reported in terms of fidelity  $\bar{F}$ , that is, the probability that Bob’s qubit, described by the density matrix  $\rho_{\text{out}}$ , successfully passes an analyser testing that it is indeed in the state  $\Psi_{\text{Alice}}$  prepared by Alice, averaged over all possible  $\Psi_{\text{Alice}}$ :

$$\bar{F} = \int \langle \Psi_{\text{Alice}} | \rho_{\text{out}} | \Psi_{\text{Alice}} \rangle d\Psi_{\text{Alice}} \quad (6)$$

The linearity of quantum mechanics implies that

$$\bar{F} = \frac{2}{3}F_{\text{equator}} + \frac{1}{3}F_{\text{poles}} \quad (7)$$

where  $F_{\text{equator}}$  and  $F_{\text{poles}}$  are the averaged fidelities for the equatorial and pole states, respectively.

To measure the teleportation fidelity  $F_{\text{equator}}$  of the equatorial states we scanned the phase  $\beta$  in Bob’s interferometer. This results in the normalized coincidence count rate:

$$R_C = \frac{1 - V \cos(\alpha + \beta)}{2} \quad (8)$$

corresponding to Bob’s state  $\rho_{\text{out}} = V|\Psi_{\text{Alice}}\rangle\langle\Psi_{\text{Alice}}| + (1 - V)(1/2)$ , where  $V$  is the visibility, which can theoretically reach the value of 1. Accordingly, the fidelity equals 1 with probability  $V$  and equals  $1/2$  with probability  $1 - V$ , hence  $F_{\text{equator}} = (1 + V)/2$ . Fig. 4a shows a good result leading to a fidelity of  $(85 \pm 2.5)\%$ . By performing repeatedly many experiments over a few weeks with different phases  $\alpha$ , we typically obtain fidelities around  $(80.5 \pm 2.5)\%$ .

The preparation of the two other states, represented by the north and south poles, implies the use of a variable coupler at settings of 0% and 100%, respectively. We realize this by using two different fibres of appropriate lengths. For the measurement, Bob uses only one fibre and looks for detections at appropriate times. As shown in equation (4), when Alice sends such a state, Bob receives the orthogonal state, that is, he should bit-flip his qubit to recover Alice’s state. The corresponding fidelity is the probability of detecting the right state when measuring in the north–south basis,  $F_{\text{poles}} = R_{\text{correct}}/(R_{\text{correct}} + R_{\text{wrong}})$  (Fig. 4b). The measured fidelity for the  $|1,0\rangle$  input state is  $(77 \pm 3)\%$  and for the  $|0,1\rangle$  input state  $(88 \pm 3)\%$ . Accordingly the mean value is  $F_{\text{poles}} = (82.5 \pm 3)\%$ .

From these results, we conclude that the overall mean fidelity is  $\bar{F} = (81.2 \pm 2.5)\%$  (equation (7)). This value is six standard deviations above the maximum fidelity of 66.7% achievable with the best protocol using no entanglement<sup>28</sup>.

The difference between our experimental results and the ideal theoretical case could be due to various imperfections. First, our Bell-state measurement is not perfect; although we tried to detect only the events when there is only one photon in each mode, there is still an 11% chance that we make a spurious coincidence. The value can be found in the noise of the teleportation of the  $|0,1\rangle$  input state, which is essentially due to the creation of double entangled pairs. The fidelity might also be reduced owing to different polarization or spectra of the two photons when arriving at the beam-splitter, or to remaining temporal distinguishability. Second, the creation and analysis of the qubits is not perfect<sup>24</sup>. Third, detector dark counts also reduce the measured fidelity. Last, one notes that teleportation occurs only when there is a projection onto the  $|\Psi^-\rangle$  state, and that only one-eighth of the qubits sent by Alice are teleported: this renders our realization probabilistic, even assuming perfect detectors. This is a drawback from a fundamental point of view. However, if

quantum teleportation were used as a quantum relay (see Fig. 5) in quantum cryptography, then the probabilistic nature of our teleportation scheme would only affect the count rate, not the quality of the quantum relay. Our scheme would be useful for this application. □

Received 19 September; accepted 13 December 2002; doi:10.1038/nature01376.

1. Bennett, C. H. *et al.* Teleporting an unknown quantum state via dual classical and Einstein-Podolsky-Rosen channels. *Phys. Rev. Lett.* **70**, 1895–1899 (1993).
2. Boschi, D., Branca, S., De Martini, F., Hardy, L. & Popescu, S. Experimental realization of teleporting an unknown pure quantum state via dual classical and Einstein-Podolsky-Rosen channels. *Phys. Rev. Lett.* **80**, 1121–1125 (1998).
3. Bouwmeester, D. *et al.* Experimental quantum teleportation. *Nature* **390**, 575–579 (1997).
4. Nielsen, M. A., Knill, E. & Laflamme, R. Complete quantum teleportation using nuclear magnetic resonance. *Nature* **396**, 52–55 (1998).
5. Kim, Y.-H., Kulik, S. P. & Shih, Y. Quantum teleportation of polarization state with a complete Bell state measurement. *Phys. Rev. Lett.* **86**, 1370–1373 (2001).
6. Lombardi, E., Sciarrino, F., Popescu, S. & De Martini, F. Teleportation of a vacuum–one-photon qubit. *Phys. Rev. Lett.* **88**, 070402 (2002).
7. Jennewein, T., Weihs, G., Pan, J.-W. & Zeilinger, A. Experimental nonlocality proof of quantum teleportation and entanglement swapping. *Phys. Rev. Lett.* **88**, 017903 (2002).
8. Furusawa, A. *et al.* Unconditional quantum teleportation. *Science* **282**, 706–709 (1998).
9. Babichev, S. A., Ries, J., Lvovsky, A. I. Quantum scissors: teleportation of single-mode optical states by mean of a nonlocal single photon. Preprint quant-ph/0208066 at (<http://xxx.lanl.gov>) (2002).
10. Bowen, W. P. *et al.* Experimental investigation of continuous variable quantum teleportation. Preprint quant-ph/0207179 at (<http://xxx.lanl.gov>) (2002).
11. Gisin, N., Ribordy, G., Tittel, W. & Zbinden, H. Quantum cryptography. *Rev. Mod. Phys.* **74**, 145–195 (2002).
12. Waks, E., Zeevi, A. & Yamamoto, Y. Security of quantum key distribution with entangled photons against individual attacks. *Phys. Rev. A* **65**, 052310 (2002).
13. Jacobs, B. C., Pittman, T. B. & Franson, J. D. Quantum relays and noise suppression using linear optics. *Phys. Rev. A* **66**, 052307 (2002).
14. Gottesman, D. & Chuang, I. L. Demonstrating the viability of universal quantum computation using teleportation and single-qubit operations. *Nature* **402**, 390–393 (1999).
15. Briegel, H.-J., Dur, W., Cirac, J. I. & Zoller, P. Quantum repeaters: The role of imperfect local operations in quantum communication. *Phys. Rev. Lett.* **81**, 5932–5935 (1998).
16. Zukowski, M., Zeilinger, A., Horne, M. A. & Ekert, A. K. “Event-ready-detectors” Bell experiment via entanglement swapping. *Phys. Rev. Lett.* **71**, 4287–4290 (1993).
17. Pan, J.-W., Bouwmeester, D., Weinfurter, H. & Zeilinger, A. Experimental entanglement swapping: Entangling photons that never interacted. *Phys. Rev. Lett.* **80**, 3891–3894 (1998).
18. Lütkenhaus, N., Calsamiglia, J. & Suominen, K.-A. Bell measurements for teleportation. *Phys. Rev. A* **59**, 3295–3300 (1999).
19. Braunstein, S. L. & Kimble, H. J. Teleportation of continuous quantum variables. *Phys. Rev. Lett.* **80**, 869–872 (1998).
20. Tittel, W. & Weihs, G. Photonic entanglement for fundamental tests and quantum communication. *Quant. Inf. Comput.* **1**, 3–56 (2001).
21. Brendel, J., Tittel, W., Zbinden, H. & Gisin, N. Pulsed energy-time entangled twin-photon source for quantum communication. *Phys. Rev. Lett.* **82**, 2594–2597 (1999).
22. Thew, R. T., Tanzilli, S., Tittel, W., Zbinden, H. & Gisin, N. Experimental investigation of the robustness of partially entangled photons over 11 km. *Phys. Rev. A* **66**, 062304 (2002).
23. De Riedmatten, H., Marcikic, I., Tittel, W., Zbinden, H. & Gisin, N. Quantum interferences with photon pairs created in spatially separated sources. *Phys. Rev. A* (in the press); preprint quant-ph/0208174 at (<http://xxx.lanl.gov>) (2002).
24. Marcikic, I., De Riedmatten, H., Tittel, W., Zbinden, H. & Gisin, N. Femtosecond time-bin entangled qubits for quantum communication. *Phys. Rev. A* **66**, 062308 (2002).
25. Lamas-Linares, A., Howell, J. C. & Bouwmeester, D. Stimulated emission of polarization-entangled photons. *Nature* **412**, 887–890 (2001).
26. Owens, P. C. M., Rarity, J. G., Tapster, P. R., Knight, D. & Townsend, P. D. Photon counting with passively quenched germanium avalanche. *Appl. Opt.* **33**, 6895–6901 (1994).
27. Stucki, D., Ribordy, G., Stefanov, A. & Zbinden, H. Photon counting for quantum key distribution with Peltier cooled InGaAs/InP APD's. *J. Mod. Opt.* **48**, 1967–1981 (2001).
28. Massar, S. & Popescu, S. Optimal extraction of information from finite quantum ensembles. *Phys. Rev. Lett.* **74**, 1259–1263 (1995).
29. Tittel, W., Brendel, J., Zbinden, H. & Gisin, N. Quantum cryptography using entangled photons in energy-time Bell states. *Phys. Rev. Lett.* **84**, 4737–4740 (2000).
30. De Riedmatten, H., Marcikic, I., Zbinden, H. & Gisin, N. Creating high dimensional entanglement using mode-locked laser. *Quant. Inf. Comput.* **2**, 425–433 (2002).
31. Grangier, P., Levenson, J. A. & Poizat, J.-P. Quantum non-demolition measurements in optics. *Nature* **396**, 537–542 (1998).

**Acknowledgements** We thank M. Legré for discussions, and C. Barreiro and J.-D. Gautier for technical support. Financial support by the Swiss OFES and NSF within the framework of the European IST project Qucomm and the Swiss National Center for Quantum Photonics is acknowledged. W.T. acknowledges support from the ESF Programme Quantum Information Theory and Quantum Computation (QIT).

**Competing interests statement** The authors declare that they have no competing financial interests.

**Correspondence** and requests for materials should be addressed to N.G. (e-mail: Nicolas.Gisin@Physics.Unige.ch).

## A colloidal model system with an interaction tunable from hard sphere to soft and dipolar

Anand Yethiraj\*† & Alfons van Blaaderen\*

\* *Soft Condensed Matter, Debye Institute, Utrecht University, Padualaan 5, 3584CC Utrecht, and FOM Institute for Atomic and Molecular Physics, Kruislaan 407, 1098 SJ Amsterdam, The Netherlands*

Monodisperse colloidal suspensions of micrometre-sized spheres are playing an increasingly important role as model systems to study, in real space, a variety of phenomena in condensed matter physics—such as glass transitions and crystal nucleation<sup>1–4</sup>. But to date, no quantitative real-space studies have been performed on crystal melting, or have investigated systems with long-range repulsive potentials. Here we demonstrate a charge- and sterically stabilized colloidal suspension—poly(methyl methacrylate) spheres in a mixture of cycloheptyl (or cyclohexyl) bromide and decalin—where both the repulsive range and the anisotropy of the interparticle interaction potential can be controlled. This combination of two independent tuning parameters gives rise to a rich phase behaviour, with several unusual colloidal (liquid) crystalline phases, which we explore in real space by confocal microscopy. The softness of the interaction is tuned in this colloidal suspension by varying the solvent salt concentration; the anisotropic (dipolar) contribution to the interaction potential can be independently controlled with an external electric field ranging from a small perturbation to the point where it completely determines the phase behaviour. We also demonstrate that the electric field can be used as a pseudo-thermodynamic temperature switch to enable real-space studies of melting transitions. We expect studies of this colloidal model system to contribute to our understanding of, for example, electro- and magneto-rheological fluids.

Recent advances in quantitative three-dimensional (3D) real-space analysis of the structure and dynamics of colloids have been accompanied by progress in the synthesis of model spheres with a controllable size and surface chemistry enabling the manipulation of the interaction potentials between the spheres<sup>5,6</sup>. Together with the well developed scattering techniques for studying colloidal systems<sup>7–12</sup>, this has led to new insights into the glass transition of simple glass formers<sup>2,3,12,13</sup>, crystal nucleation and growth<sup>4,7–10,14</sup>, and the role of the attractive part of interaction potentials on phase behaviour<sup>11</sup>.

The simplest colloidal model system with short-ranged repulsive interactions is either a sterically stabilized particle suspension<sup>5,14,15</sup>, or an aqueous suspension of micrometre-sized latex spheres with salt added to ensure that the inverse Debye screening length,  $1/\kappa$ , a measure for the range of the repulsion, is short;  $\kappa R = 33$  for spheres of radius  $R = 1 \mu\text{m}$  in water at a monovalent salt concentration of  $c = 0.1 \text{ mM}$ . To realize almost hard-sphere behaviour, the always-present van der Waals attractions have to be reduced by matching the index of refraction in the visible. This allows the interactions to be tuned to almost hard-sphere-like even for micrometre-sized colloids that can be quantitatively imaged in 3D by confocal microscopy. The role of gravity (far more important in colloids than in the crystallization of atomic and molecular fluids) is minimized by matching the density of the spheres and solvent. A step-up in complexity could involve either introducing a dipolar interaction, thus making the interaction anisotropic, or extending

† Present address: Department of Chemistry, 2036 Main Mall, Vancouver, British Columbia, Canada V6T 1Z1.